bioRxiv preprint doi: https://doi.org/10.1101/2022.03.26.485894; this version posted March 27, 2022. The copyright holder for this preprint (which was not certified by peer review) is the author/funder, who has granted bioRxiv a license to display the preprint in perpetuity. It is made available under aCC-BY-ND 4.0 International license.

Dynamic analysis of sequestration-based feedbacks in cellular and biomolecular circuits

Supravat Dey[1], Cesar A. Vargas-Garcia[2] and Abhyudai Singh [3]

***Abstract*— Nonlinear feedback controllers are ubiquitous features of biological systems at different scales. A key motif arising in these systems is a sequestration-based feedback. As a physiological example of this type of feedback architecture, platelets (specialized cells involved in blood clotting) differentiate from stem cells, and this process is activated by a protein called Thrombopoietin (TPO). Platelets actively sequester and degrade TPO, creating negative feedback whereby any depletion of platelets increases the levels of freely available TPO that upregulates platelet production. We show similar examples of sequestration-based feedback in intracellular biomolecular circuits involved in heat-shock response and microRNA regulation. Our systematic analysis of this feedback motif reveals that platelets induced degradation of TPO is critical in enhancing system robustness to external disturbances. In contrast, reversible sequestration of TPO without degradation results in poor robustness to disturbances. We develop exact analytical results quantifying the limits to which the sensitivity to disturbances can be attenuated by sequestration-based feedback. Next, we consider the stochastic formulation of the circuit that takes into account low-copy number fluctuations in feedback components. Interestingly, our results show that the extent of random fluctuations are enhanced with increasing feedback strength, but can exhibit local maxima and minima across parameter regimes. In summary, our systematic analysis highlights design principles for enhancing the robustness of sequestration-based feedback mechanisms to external disturbances and inherent noise in molecular counts.**

I. Introduction

As in engineering, feedback regulation forms the key basis of homeostasis in physiological and cellular systems. Perhaps the simplest example of this is seen in the regulation of gene expression, where a transcription factor binds to the promoter of its own gene to modulate transcriptional activity. Such forms of gene autoregulation are key motifs in gene regulatory networks [1], and have been thoroughly investigated using a combination of mathematical and experimental tools. These studies highlight how gene autoregulation can alter response times [2]–[4], attenuate the impacts of stochasticity [5]–[18], and alter the system's information capacity [19]. There is a growing appreciation of similar autoregulatory feedbacks at play in cell populations controlling their density through extracellularly secreted factors [20]–[23], and neurotransmitter binding to autoreceptors on neuronal membranes to maintain homeostatic activity [24]–[27].

[1]Supravat Dey is with the Department of Physics, SRM University -AP, Amaravati, Andhra Pradesh 522502, India. supravat.dey@gmail.com, [2]Abhyudai Singh is with the Departments of Electrical and Computer Engineering, Biomedical Engineering at the University of Delaware, Newark, DE 19716, USA. absingh@udel.edu,[3]Cesar Vargas-Garcia is with Corporación Colombiana de Investigación Agropecuaria - Agrosavia, Mosquera, Colombia. caugusto.vargas@gmail.com

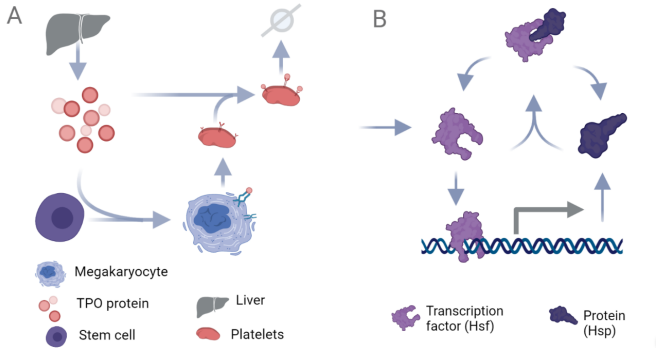

Fig. 1. **Examples of sequestration-based feedback in physiology and cellular responses.** A: The differentiation of stem cells into megakaryocytes and platelets is driven by a protein called Thrombopoietin (TPO) that is produced from the liver. Megakaryocytes/platelets sequester and degrade TPO implementing a feedback mechanism where depletion of platelets increases their synthesis via an upregulation in freely available TPO [28]–[30]. B: The biomolecular circuit orchestrating the cellular heat-shock response. The heat-shock protein (Hsp) binds and sequesters the heat-shock factor (Hsf), and free Hsf proteins upregulate the synthesis of Hsp.

In this study, we go beyond autoregulation to consider a nonlinear feedback system that we refer to as *sequestration-based feedback*. It can represent by the following system of chemical reactions

$$\emptyset \rightarrow X_f, \quad X_f \rightarrow Y_f + X_f, \quad Y_f + X_f \leftrightarrow C \tag{1}$$

where a species X_f is produced constitutively at a constant rate and activates the production of species Y_f. Y_f reversible binds to X_f sequestering it in a complex C. In essence, an increase in Y_f levels results in a downregulation of its synthesis through sequestration of its activator X_f. Several examples of this can be seen in biology as illustrated in Fig. 1. As a physiological example, hematopoietic stem cells residing in the bone marrow are induced to differentiate into platelets (Y_f) by a protein called Thrombopoietin (X_f). However, megakaryocytes (precursor cells that produce platelets) and platelets actively sequester Thrombopoietin (TPO) and degrade it. Thus, depletion of platelets in response to injury leads to an upregulation in platelet synthesis via an increase in free TPO levels [28]–[30]. While the differentiation of stem cells into platelets is a complex process occurring through several intermediate states, for modeling simplicity we consider platelet synthesis occurring in a single TPO-dependent rate. A key focus is to understand how platelet-induced degradation of sequestered TPO can enhance the system's robustness to fluctuations in platelet demand.

A classic biomolecular example of sequestration-based

bioRxiv preprint doi: https://doi.org/10.1101/2022.03.26.485894; this version posted March 27, 2022. The copyright holder for this preprint (which was not certified by peer review) is the author/funder, who has granted bioRxiv a license to display the preprint in perpetuity. It is made available under aCC-BY-ND 4.0 International license.

TABLE I

DIFFERENT CHEMICAL REACTIONS CONSTITUTING THE SEQUESTRATION-BASED FEEDBACK ALONG WITH THEIR NET RATES

Reaction	Net rate	Comment
$\emptyset \to X_f$	k_x	Synthesis of Thrombopoietin (TPO)
$X_f \to Y_f + X_f$	$k_y x_f$	Production of platelets by free TPO
$Y_f + X_f \to C$	$k_b x_f y_f$	Binding of TPO to platelets
$C \to Y_f + X_f$	$k_u c$	Unbinding of TPO from platelets
$C \to Y_f$	$\gamma_i c$	Platelet-induced decay of TPO
$C \to \emptyset$	$\gamma_y c$	Degradation of TPO-bound platelets
$Y_f \to \emptyset$	$\gamma_y y_f$	Degradation of TPO-unbound platelets
$X_f \to \emptyset$	$\gamma_x x_f$	Degradation of free TPO

feedback is the cellular heat-shock response (Fig. 1B), where heat-shock protein (Y_f) sequesters the heat-shock factor (X_f). Exposure to heat denatures proteins, and heat-shock proteins (Hsp) are chaperones that assist in protein refolding. The binding of Hsp to client proteins results in an increase in free heat-shock factor (Hsf) levels as there is less free Hsp available to bind to Hsf. Hsf is a transcription factor (TF) that once released from the complex binds to the Hsp gene promoter to upregulate its synthesis closing the feedback loop [31]–[33].

Other examples of sequestration-based feedback include biomolecular circuits involved in controlling rDNA repeats [34] and the growing evidence of feedback between specific microRNAs and TFs. In the latter example, TFs activate the synthesis of microRNAs and the feedback is implemented by having the microRNA bind and sequester the TF mRNA to turn off TF synthesis [35], [36]. It is important to point out that a special case of sequestration-based feedback is the antithetic integral feedback that has been recently studied [37]–[40] and also experimentally implemented via synthetic circuits [41], [42]. Such forms of integral feedback play a vital role in the adaptation of biological processes to changes in input stimuli [43]–[46].

Overall, the paper is organized as follows. In Section II, we develop a nonlinear dynamical model for the sequestration-based feedback. We study in Section III how sensitive the total platelet abundances are to fluctuation in platelet consumption rate. Our analysis derives fundamental limits to which this sensitivity can be reduced and finds platelet-induced TPO decay to be critical for robust buffering. In Section IV, we turn to a stochastic formulation of the heat-shock response circuit and investigate feedback performance in the presence of inherent stochasticity in gene expression.

II. DETERMINISTIC MODEL FORMULATION

The system of chemical events that implement the sequestration-based feedback is shown in Table I along with the net rates with which these reactions occur per unit time. Here capital letters denotes species:

- X_f – free Thrombopoietin (TPO) not bound to platelets
- Y_f – free platelets not bound to TPO
- C – platelets bound to TPO.

The corresponding small letters $x_f(t)$, $y_f(t)$, $c(t)$ represent the concentration of species at time t. To be physiologically relevant, these state variables can only take positive real values. Combining the rates of production and loss for each chemical species results in the following nonlinear dynamical system describing the time evolution of concentrations

$$\frac{dx_f}{dt} = k_x - \gamma_x x_f - k_b y_f x_f + k_u c \tag{2a}$$

$$\frac{dy_f}{dt} = k_y x_f - \gamma_y y_f + \gamma_i c - k_b y_f x_f + k_u c \tag{2b}$$

$$\frac{dc}{dt} = k_b y_f x - k_u c - \gamma_y c - \gamma_i c \tag{2c}$$

where k_x is the constitutive rate of TPO synthesis from the liver. Free TPO molecules drive the synthesis of new platelets with rate $k_y x_f$, and we refer to k_y as the *platelet activation rate*. Binding and unbinding of TPO to platelets occurs with rates k_b and k_u, respectively, as per mass-action kinetics. An important parameter representing platelet-induced degradation of bound TPO is γ_i that converts a TPO-bound platelet back into a free platelet ($C \to Y_f$ reaction in Table I). Later on we will specifically investigate the role of γ_i in platelet homeostasis. Finally, free TPO is degraded with rate γ_x, and γ_y is the rate of consumption of platelets that is assumed to be the same irrespective of whether it's bound or unbound to TPO. Here $1/\gamma_y$ is average lifespan of an individual platelet that has been measured to be ≈ 1 week in humans [47]–[49].

Since we are primarily interested in the total amount of platelets, (2) is transformed to

$$\frac{dx_T}{dt} = k_x - \gamma_x x_f - (\gamma_y + \gamma_i) c \tag{3a}$$

$$\frac{dy_T}{dt} = k_y x_f - \gamma_y y_T \tag{3b}$$

$$\frac{dc}{dt} = k_b y_f x_f - k_u c - \gamma_y c - \gamma_i c \tag{3c}$$

by considering a change of variables

$$x_T = x_f + c, \qquad y_T = y_f + c, \tag{4}$$

where x_T and y_T denote the total (bound plus unbound) level of TPO and platelets, respectively. In the limit of fast binding/unbinding (i.e., $k_u \to \infty$ and $k_b \to \infty$) for a given dissociation constant

$$k_d = \frac{k_u}{k_b}, \tag{5}$$

the free platelet and TPO concentrations rapidly equilibrate such that

$$\begin{aligned} k_b y_f x_f = k_u c \implies & y_f x_f = k_d c \\ \implies & (y_T - c)(x_T - c) = k_d c. \end{aligned} \tag{6}$$

bioRxiv preprint doi: https://doi.org/10.1101/2022.03.26.485894; this version posted March 27, 2022. The copyright holder for this preprint (which was not certified by peer review) is the author/funder, who has granted bioRxiv a license to display the preprint in perpetuity. It is made available under aCC-BY-ND 4.0 International license.

Thus, given the total platelet and TPO levels (y_T and x_T) at any time instant, solving (6) yields the bound platelet level

$$c(x_T,y_T)=\frac{k_d+x_T+y_T-\sqrt{(k_d+x_T+y_T)^2-4x_Ty_T}}{2} \quad (7)$$

resulting from fast binding and unbinding processes. Before proceeding further, we highlight key properties of this continuously differentiable function $c(x_T,y_T)$, $\forall x_T,y_T\geq 0$:

- $c(0,y_T)=0$ and $c(x_T,0)=0$.
- $0\leq c(x_T,y_T)\leq$ Minimum of x_T and y_T.
- $c(x_T,y_T)$ monotonically increases with respect to both arguments with bounded slope (proof in Appendix):

$$0\leq\frac{\partial c(x_T,y_T)}{\partial x_T}\leq 1,\quad 0\leq\frac{\partial c(x_T,y_T)}{\partial y_T}\leq 1. \quad (8)$$

- In the limit of rapid TPO dissociation (i.e., no binding of TPO to platelets)

$$\lim_{k_d\to\infty} c(x_T,y_T)=0 \quad (9)$$

Exploiting this timescale separation, the original model (3) is now reduced to a two-dimensional model

$$\frac{dx_T}{dt}=k_x-\gamma_x(x_T-c(x_T,y_T))-(\gamma_y+\gamma_i)c(x_T,y_T) \quad (10a)$$
$$\frac{dy_T}{dt}=k_y(x_T-c(x_T,y_T))-\gamma_y y_T. \quad (10b)$$

Having formulated the model we present our first result on the uniqueness and stability of its equilibrium point.

Theorem: The two-dimensional nonlinear system (10) has a unique *asymptotically stable* equilibrium given by

$$y_T^*=\frac{k_y\left(k_x-\gamma_x k_d+\sqrt{\gamma_x^2k_d^2+2k_d\left(\gamma_x+2\left(\frac{\gamma_i}{\gamma_y}+1\right)k_y\right)k_x+k_x^2}\right)}{2(\gamma_x\gamma_y+(\gamma_i+\gamma_y)k_y)} \quad (11a)$$

$$x_T^*=\frac{y_T^*\gamma_y}{k_y}+\frac{y_T^*}{(k_dk_y+\gamma_y y_T^*)}. \quad (11b)$$

Proof: Solving the nonlinear system (10) at steady-state yields a unique equilibrium point given by (11). As expected, in the limit of no TPO binding to platelets this equilibrium reduces to

$$\lim_{k_d\to\infty} y_T^*=\frac{k_yk_x}{\gamma_x\gamma_y},\quad \lim_{k_d\to\infty} x_T^*=\frac{\gamma_y y_T^*}{k_y}=\frac{k_x}{\gamma_x}. \quad (12)$$

Linearizing the nonlinear systems around (11) yields the following Jacobian matrix

$$A=\begin{bmatrix} a_{11} & a_{12}\\ a_{21} & a_{22}\end{bmatrix}$$

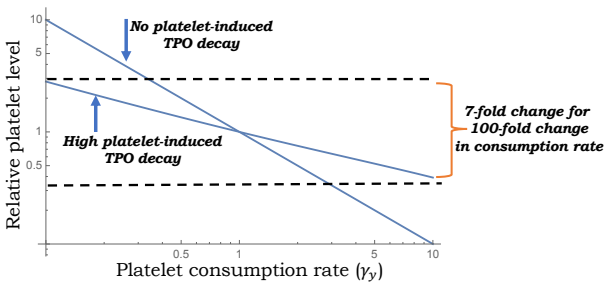

Fig. 2. **Platelet-induced TPO decay buffers platelet abundance to increase in consumption rates**. Plot of total platelet abundance y_T^* as given by (11) for varying consumption rate γ_y. A hundred-fold change in γ_y results in a hundred-fold ($\gamma_i=0$) and seven-fold ($\gamma_i=50$) change in y_T^*. Other parameter taken as $k_y=10$, $k_d=1$ and k_x was varied so as to have $y_T^*=1$ when $\gamma_y=1$. All timescales are normalized to TPO lifespan that results in $\gamma_x=1$, and both TPO/platelet levels have arbitrary units.

$$a_{11}=-\gamma_x+\frac{\partial c(x_T,y_T)}{\partial x_T}|_{x_T=x_T^*,y_T=y_T^*}(\gamma_x-\gamma_y-\gamma_i) \quad (13a)$$
$$a_{12}=\frac{\partial c(x_T,y_T)}{\partial y_T}|_{x_T=x_T^*,y_T=y_T^*}(\gamma_x-\gamma_y-\gamma_i) \quad (13b)$$
$$a_{21}=k_y-k_y\frac{\partial c(x_T,y_T)}{\partial x_T}|_{x_T=x_T^*,y_T=y_T^*} \quad (13c)$$
$$a_{22}=-k_y\frac{\partial c(x_T,y_T)}{\partial y_T}|_{x_T=x_T^*,y_T=y_T^*}-\gamma_y. \quad (13d)$$

The trace of the A matrix is given by

$$\begin{aligned}\text{Trace } A=&-\gamma_x\left(1-\frac{\partial c(x_T,y_T)}{\partial x_T}|_{x_T=x_T^*,y_T=y_T^*}\right)\\&-\frac{\partial c(x_T,y_T)}{\partial x_T}|_{x_T=x_T^*,y_T=y_T^*}(\gamma_y+\gamma_i)\\&-k_y\frac{\partial c(x_T,y_T)}{\partial y_T}|_{x_T=x_T^*,y_T=y_T^*}-\gamma_y<0\end{aligned} \quad (14)$$

which is strictly negative, as from (8), $c(x_T,y_T)$ is a monotonically increasing function in both arguments with

$$1-\frac{\partial c(x_T,y_T)}{\partial x_T}\geq 0. \quad (15)$$

Thus, each of the three terms in (14) are individually negative, making the trace negative. Using a similar argument we can see that all the three terms making up the following determinant of the A matrix

$$\begin{aligned}\text{Det } A=&\frac{\partial c(x_T,y_T)}{\partial x_T}|_{x_T=x_T^*,y_T=y_T^*}\gamma_y(\gamma_y+\gamma_i)\\&+\gamma_y\gamma_x\left(1-\frac{\partial c(x_T,y_T)}{\partial x_T}|_{x_T=x_T^*,y_T=y_T^*}\right)\\&+k_y\frac{\partial c(x_T,y_T)}{\partial y_T}|_{x_T=x_T^*,y_T=y_T^*}(\gamma_y+\gamma_i)>0\end{aligned} \quad (16)$$

are individually positive, hence implying a positive determinant. For a 2×2 A matrix, a negative trace and a positive determinant are *necessary and sufficient* for asymptotic stability [50]. We also note that

$$0\leq x_T\leq\frac{k_x}{\min\{\gamma_x,\gamma_y\}},\quad 0\leq y_T\leq\frac{k_x}{\min\{\gamma_x,\gamma_y\}}\frac{k_y}{\gamma_y} \quad (17)$$

bioRxiv preprint doi: https://doi.org/10.1101/2022.03.26.485894; this version posted March 27, 2022. The copyright holder for this preprint (which was not certified by peer review) is the author/funder, who has granted bioRxiv a license to display the preprint in perpetuity. It is made available under aCC-BY-ND 4.0 International license.

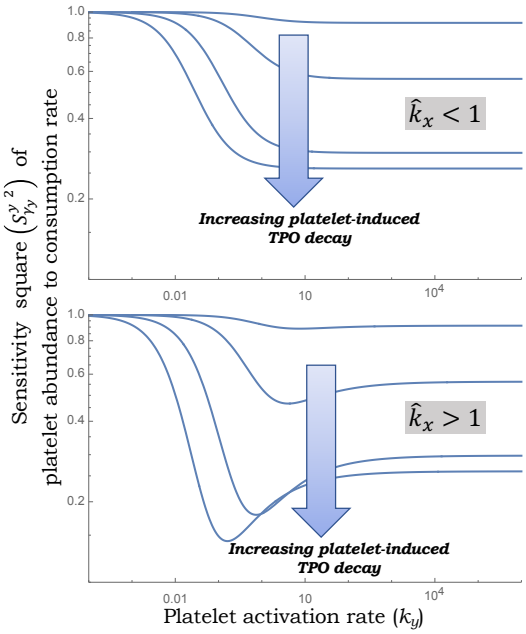

Fig. 3. **Sensitivity of platelet abundance to consumption rate is minimized at an optimal activation rate**. Plot of the square of (24) as a function of k_y for $\hat{k}_x < 1$ (top) and $\hat{k}_x > 1$ (bottom). Other parameters take an $\gamma_x = \gamma_y = k_d = 1$. The four different curves correspond to $\gamma_i = 0.1, 1, 10, 50$.

is an invariant set, i.e., trajectories starting outside the set will enter it in finite time and remain there. More specifically, if

$$x_T > \frac{k_x}{\min\{\gamma_x, \gamma_y\}} \implies \frac{dx_T}{dt} < 0. \tag{18}$$

This can be seen by considering two cases, first if $\gamma_y > \gamma_x$, then the right-hand-side of (10a) is

$$k_x - \gamma_x x_T - (\gamma_y - \gamma_x) c(x_T, y_T) - \gamma_i c(x_T, y_T) < 0 \tag{19}$$

if $x_T > \frac{k_x}{\gamma_x}$. Secondly if $\gamma_y < \gamma_x$, then the right-hand-side of (10a) can be rewritten as

$$k_x - \gamma_y x_T - (\gamma_x - \gamma_y)(x_T - c(x_T, y_T)) - \gamma_i c(x_T, y_T) < 0 \tag{20}$$

if $x_T > \frac{k_x}{\gamma_y}$ as $c(x_T, y_T) \leq x_T$. Once the trajectory reaches $x_T \leq \frac{k_x}{\min\{\gamma_x, \gamma_y\}}$, then from (10b) if

$$y_T > \frac{k_x}{\min\{\gamma_x, \gamma_y\}} \frac{k_y}{\gamma_y} \implies \frac{dy_T}{dt} < 0. \tag{21}$$

III. Sensitivity Analysis

Having determined the model's equilibrium, we next study the sensitivity of the total platelet abundance y_T^* to the consumption rate γ_y which can dramatically go up in response to injury. This can be quantified by the dimensionless log sensitivity

$$S^y_{\gamma_y} := \frac{\partial \ln y_T^*}{\partial \ln \gamma_y} = \frac{\gamma_y}{y_T^*} \frac{\partial y_T^*}{\partial \gamma_y}. \tag{22}$$

From (11), in the absence of platelet-induce TPO decay ($\gamma_i = 0$) the total platelet abundance

$$\lim_{\gamma_i \to 0} y_T^* = \frac{k_y \left(k_x - \gamma_x k_d + \sqrt{\gamma_x^2 k_d^2 + 2k_d(\gamma_x + 2k_y) k_x + k_x^2}\right)}{2\gamma_y(\gamma_x + k_y)} \tag{23}$$

is inversely proportional to γ_y that results in $S^y_{\gamma_y} = -1$. Thus, a hundred-fold increase in γ_y results in a hundred-fold decrease in platelet abundance (Fig. 2). In contrast, presence of platelet-induced TPO decay ($\gamma_i > 0$) can significantly buffer this decrease by making y_T^* less sensitive to γ_y (Fig. 2). Are their limits to which sensitivity can be reduced and how does this limit depend on γ_i?

To quantify the fundamental limit to which sensitivity can be suppressed, we derive the following general formula for $S^y_{\gamma_y}$ from (11)

$$S^y_{\gamma_y} = \tag{24}$$

$$-1 + \frac{\gamma_i k_y \left(1 + \frac{k_x - k_d \gamma_x}{\sqrt{\gamma_x^2 k_d^2 + 2k_d\left(\gamma_x + 2\left(\frac{\gamma_i}{\gamma_y} + 1\right)k_y\right)k_x + k_x^2}}\right)}{2(\gamma_i k_y + \gamma_y(\gamma_x + k_y))}. \tag{25}$$

Our analysis of this formula reveals that it can either vary monotonically or non-monotonically with respect to the platelet activation rate k_y. To see this, we first define the dimensionless constant

$$\hat{k}_x = \frac{k_x}{\gamma_x k_d}, \tag{26}$$

where recall from (12) that k_x/γ_x is the total TPO level in the absence of any binding to platelets. When $\hat{k}_x \leq 1$, then $S^y_{\gamma_y}$ monotonically decreases with increasing activation rate k_y (Fig. 3; top) with the following limits

$$\lim_{k_y \to 0} S^y_{\gamma_y} = -1 \tag{27a}$$

$$\lim_{k_y \to \infty} S^y_{\gamma_y} = -\frac{\gamma_i + 2\gamma_y}{2(\gamma_i + \gamma_y)}. \tag{27b}$$

Thus, in this regime, (27b) gives the fundamental limit of sensitivity repressions with $S^y_{\gamma_y}$ approaching $-1/2$ as $\gamma_i \to \infty$.

Interestingly, when $\hat{k}_x > 1$, y_T^* varies non-monotonically with k_y and is minimized at an intermediate value of the platelet activation rate (Fig. 3; bottom). Please note that since $S^y_{\gamma_y}$ is negative, Fig. 3 plots the square $\left(S^y_{\gamma_y}\right)^2$. In the case of $\hat{k}_x > 1$, our results show that the optimal reduction of sensitivity occurs when

$$k_y = \frac{\gamma_y \gamma_x \left(1 + \hat{k}_x^2\right)}{(\gamma_i + \gamma_y)\left(\sqrt{\hat{k}_x} - 1\right)^2 \sqrt{\hat{k}_x}} \tag{28}$$

and the corresponding sensitivity is

$$S^y_{\gamma_y} = -\frac{\gamma_y}{\gamma_i + \gamma_y} - \frac{2\gamma_i \sqrt{\hat{k}_x}}{(\gamma_i + \gamma_y)\left(1 + \sqrt{\hat{k}_x}\right)^2}. \tag{29}$$

bioRxiv preprint doi: https://doi.org/10.1101/2022.03.26.485894; this version posted March 27, 2022. The copyright holder for this preprint (which was not certified by peer review) is the author/funder, who has granted bioRxiv a license to display the preprint in perpetuity. It is made available under aCC-BY-ND 4.0 International license.

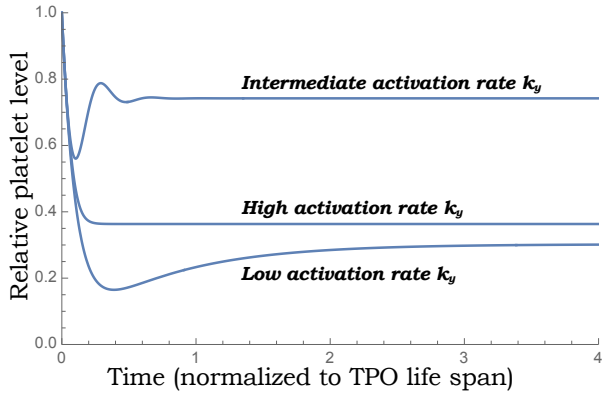

Fig. 4. **Optimally set activation rate k_y yields minimal depression of platelet count in response to increased consuption**. The platelet abundance $y_T(t)$ as obtained by solving the nonlinear system (10) for a ten-fold change in γ_y from 1 to 10. Other parameters taken as $\gamma_i = 100$, $k_d = 0.1$, $k_x = 100$ and $\gamma_x = 1$. The intermediate activation rate corresponds to k_y chosen as per (28), and other curves were generated assuming a hundred-fold higher or lower value than (28).

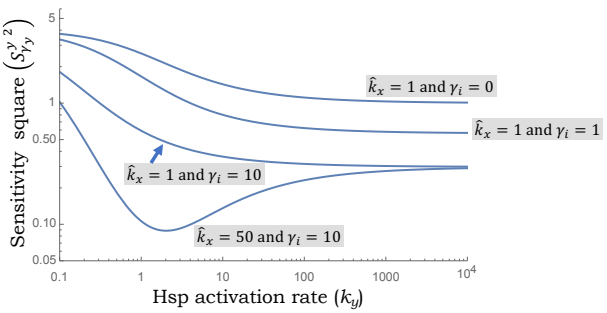

Fig. 5. **Sensitivity of total heat-shock protein abundance to growth rate is minimized at an optimal hsp activation rate**. Plot of the square of the sensitivity $S^y_{\gamma_y}$ for the biomolecular sequestration-based feedback describing the heat-shock response (Fig. 1B). Here $\gamma_x = \gamma_y$, where γ_y is the cellular growth rate. As in Fig. 3, other parameters are taken as $\gamma_x = \gamma_y = k_d = 1$.

In the limit $\hat{k}_x \gg 1$, the optimal value of k_y and the corresponding minimal sensitivity simplify to

$$k_y \approx \frac{\gamma_y \gamma_x \sqrt{\hat{k}_x}}{\gamma_i + \gamma_y}, \quad S^y_{\gamma_y} \approx -\frac{\gamma_y}{\gamma_i + \gamma_y}, \tag{30}$$

respectively. Note that this limit of sensitivity suppression is inversely related to γ_i, thus can be made arbitrarily small by arbitrarily enhancing the platelet-induced decay rate. The effect of this sensitivity reduction can also be seen in the dynamical response of platelet abundance to a step increase in the consumption rate. (Fig. 4). The optimally chosen value of k_y as per (28) results in a lower depression in $y_T(t)$ as compared to higher and lower values of k_y (Fig. 4).

IV. Biomolecular sequestration-based feedback

We next consider a biomolecular example of sequestration-based feedback as depicted in Fig. 1B. More specifically, the heat-shock protein (Hsp) binds and sequester the heat-shock factor (Hsf), and free Hsf proteins activate the production of Hsp by enhancing its gene's transcription [31], [32]. The deterministic model formulation is exactly similar to (2) but with redefined species

- X_f – free Hsf protein not bound to Hsp
- Y_f – free Hsp protein not bound to Hsf
- C – Hsp protein bound to Hsf.

Moreover, we now refer to k_y and γ_i as the *hsp activation rate* and *hsf-induced hsf decay rate*. Given that these proteins are fairly stable with long half-lives, the decay in their concentrations is primarily from cellular growth during the cell cycle. Towards that end,

$$\gamma_x = \gamma_y \tag{31}$$

where γ_y is the cellular growth rate. *How robust are total Hsp levels to growth rate fluctuations?*

A formula for sensitivity $S^y_{\gamma_y}$ can again be obtained from (11) which is slightly different from that obtained earlier for the TPO-platelet circuit where γ_x and γ_y were independent parameters. However, this formula shows qualitatively similar behavior with

$$\lim_{\gamma_i \to \infty} S^y_{\gamma_y} \to -\frac{1}{2}. \tag{32}$$

A plot of $S^y_{\gamma_y}$ with respect to the activation rate in Fig. 5 shows that as in Fig. 3, for small values of $\hat{k}_x$, $S^y_{\gamma_y}$ monotonically decreases with increasing k_y to reach the limit (27b). In contrast, for large values of $\hat{k}_x$, $S^y_{\gamma_y}$ shows a U-shape profile where the minimal sensitivity can be made arbitrarily close to zero by enhancing γ_i. An important quantitate difference to note is that while $S^y_{\gamma_y} > -1$ in the TPO-platelet circuit (Fig. 3), in the heat-shock system $S^y_{\gamma_y} < -1$ for certain parameter regimes (Fig. 5) implying a decay in y^*_T with an increasing growth rate that is even faster than γ_y^{-1}.

Having examined fluctuations in the growth rate, we next consider an alternative source of stochasticity in the biomolecular circuit that arises from the synthesis of gene products in bursts of transcriptional activity. We analyze the impact of such bursting on total Hsp levels in stochastically-formulated models of sequestration-based feedback.

A. Stochastic Analysis

We next consider a stochastic formulation of the chemical reaction set in Table I, where Hsf is produced in random bursts. In gene expression, such bursty synthesis is realized due to the short lifespan of mRNA compared to the corresponding protein, as in prokaryotes [51]. In eukaryotes, however, the cause of burst is usually the gene switching between active and inactive states [52]–[56]. Such bursty expressions are the major sources of large fluctuations in expression levels (gene expression noise). As Hsf activates the Hsp production, its noise propagates and makes the Hsp level highly noisy. For simplicity, we assume a simple non-bursty birth process for Hsp production.

Notation: In this formalism, $x(t)$ denotes the number of copies species X. It takes a random non-negative integer value i.e., $x(t) \in \{0,1,2,3,...\}$. We use angular brackets $\langle\cdot\rangle$ and $\overline{\langle\cdot\rangle}$ to denote the transient and steady-state expected values for the stochastic process, respectively.

bioRxiv preprint doi: https://doi.org/10.1101/2022.03.26.485894; this version posted March 27, 2022. The copyright holder for this preprint (which was not certified by peer review) is the author/funder, who has granted bioRxiv a license to display the preprint in perpetuity. It is made available under aCC-BY-ND 4.0 International license.

The probability of the Hsf and Hsp production events in infinitesimal interval $(t, t+dt]$ are given by

$$Prob(x_f \to x_f+b) = k_x \alpha(b)\, dt, \text{for } b \in \{0,1,2,3,..,\} \quad (33a)$$
$$Prob(y_f \to y_f+1) = k_y x_f\, dt, \quad (33b)$$

where $\alpha(b)$ is the burst size distribution, generally follows geometric distributions. The probability of binding and unbinding events are

$$Prob(x_f \to x_f-1, y_f \to y_f-1, c \to c+1) = k_b x_f y_f\, dt, \quad (34a)$$
$$Prob(x \to x_f+1, y_f \to y_f+1, c \to c-1) = k_u c\, dt, \quad (34b)$$

All the species decay with the same rate $\gamma_x = \gamma_y = \gamma_c$. In addition, there is a Hsp-induced Hsf degradation which occurs at rate γ_i. The probabilities of the degradation events during the infinitesimal interval are

$$Prob(x_f \to x_f-1) = \gamma_y x_f\, dt, \quad (35a)$$
$$Prob(y_f \to y_f-1) = \gamma_y y_f\, dt, \quad (35b)$$
$$Prob(c \to c-1) = \gamma_y c\, dt, \quad (35c)$$
$$Prob(y_f \to y_f+1, c \to c-1) = \gamma_i c\, dt. \quad (35d)$$

Noise in total Hsp count: We are interested in understanding fluctuations in the total Hsp count ($y_T = y_f + c$) at steady-state. The fluctuations, also known as gene expression noise, can be quantified by the Fano factor in y_T

$$F_{y_T} = \frac{\overline{\langle y_T^2 \rangle} - \overline{\langle y_T \rangle}^2}{\overline{\langle y_T \rangle}}, \quad (36)$$

where $\overline{\langle y_T \rangle}$ and $\overline{\langle y_T^2 \rangle}$ are the first and second-order moments of y_T at steady-state.

The nonlinear binding term makes the exact analytical calculation difficult. In the absence of binding, one can obtain exact analytical results using the chemical master equation framework for discrete-state continuous-time Markov processes [57]. For no binding case,

$$\overline{\langle x_f \rangle} = \overline{\langle x_T \rangle} = k_x \langle b \rangle / \gamma_y, \quad (37a)$$
$$\overline{\langle y_f \rangle} = \overline{\langle y_T \rangle} = k_y k_x \langle b \rangle / \gamma_y^2, \quad (37b)$$
$$F_{y_T} = 1 + \frac{(\langle b^2 \rangle + \langle b \rangle)\overline{\langle y_T \rangle}}{4\langle b \rangle \overline{\langle x_T \rangle}} = 1 + \frac{(\langle b^2 \rangle + \langle b \rangle) k_y}{4\langle b \rangle \gamma_y}, \quad (37c)$$

where $\langle b \rangle = \sum_i i\, \alpha(i)$ represents the average burst size and $\langle b^2 \rangle = \sum_i i^2\, \alpha(i)$. Both $\overline{\langle y_T \rangle}$ and F_{y_T} linearly depend on the activation rate k_y. The noise level also increases with the average size and width of the burst size distribution.

To analyze the noise in the presence of binding, we perform numerically exact stochastic simulations using the kinetic Monte Carlo method [58]. In Fig. 6, we plot the mean (A) and the noise behavior (B) in the total Hsp count as a function of the activation rate. For very low values of k_y ($k_y/\gamma_y \ll 1$), $\overline{\langle y_T \rangle}$ linearly increases with k_y, following the no-binding case above. For an intermediate k_y, the increase in $\overline{\langle y_T \rangle}$ becomes flat, and finally, $k_y/\gamma_y \gg 1$ the increase becomes faster again but stays well below the no-binding case due to negative feedback (Fig. 6A). The Hsp-induced Hsf decay further reduces $\overline{\langle y_T \rangle}$ and also decreases the intermediate flat region.

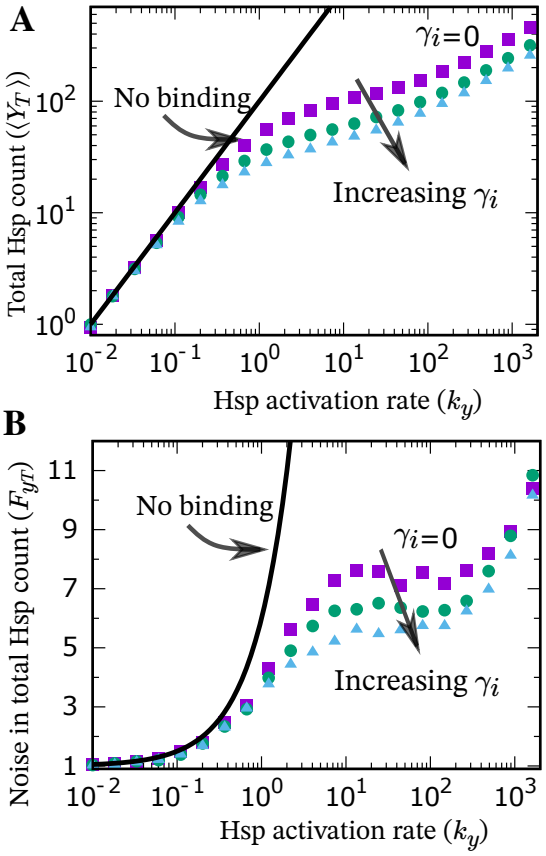

Fig. 6. **Hsp-induced Hsf degradation reduces noise in total Hsp count.** The mean (A) and the Fano factor (B) are plotted against k_y for different values of γ_i ($= 0,\ \gamma_y,\ 2\gamma_y$). The lines represent analytical results for no binding case, whereas symbols denote stochastic simulation results in the presence of binding. Parameters used: $\langle b \rangle = 10$, $k_x = 10$, $\gamma_y = 1$, $k_d = 1$ and $k_u = 40$. Our burst size distribution is a shifted geometric distribution.

Implementing the feedback through the Hsp-Hsf binding reduces the noise in the total Hsp count as compared to the no-binding case (Fig. 6B), and the hsp-induced Hsf decay decreases F_{y_T} further. Interestingly, our results show a nonmonotonicity in F_{y_T} at an intermediate value of k_y when γ_i is relatively small, and this is connected to the flattening in $\overline{\langle y_T \rangle}$ levels seen in Fig. 6A.

V. Conclusion

There is growing literature on leveraging sequestration processes for feedback control of biomolecular systems [59], [60]. Here we analyzed a sequestration-based feedback architecture illustrated in Table I that mimics homeostatic control occurring at diverse spatial scales from maintaining cell numbers in an organism to regulating intracellular concentrations of key gene products (Fig. 1). Our model presented in (2) reduce to the well-studied antithetic integral feedback in the limit $\gamma_i = \gamma_u = \gamma_y = 0$ that corresponds to X_f irreversibly binding to Y_f, and both subsequently degrading. In this case (2b) becomes

$$\frac{dy_f}{dt} = x_f(k_y - k_b y_f) \quad (38)$$

bioRxiv preprint doi: https://doi.org/10.1101/2022.03.26.485894; this version posted March 27, 2022. The copyright holder for this preprint (which was not certified by peer review) is the author/funder, who has granted bioRxiv a license to display the preprint in perpetuity. It is made available under aCC-BY-ND 4.0 International license.

and one can see the integral feedback (albeit with a time-varying coefficient x_f) that regulates y_f around its steady-state value k_y/k_b. As pointed out earlier [61], from a practical standpoint this integration is "leaky" due to the effects of dilution ($\gamma_y \neq 0$).

Our analysis of the sequestration-based feedback identified limits to which the sensitivity of total Y_f levels to its degradation rate γ_y can be reduced. The key result is presented in (29), where the absolute value of $S^y_{\gamma_y}$ reduces with increasing platelet-induced TPO degradation γ_i reaching the limits

$$S^y_{\gamma_y} \to -\frac{\gamma_y}{\gamma_i+\gamma_y}, \quad \hat{k}_x \to \infty \tag{39}$$

$$S^y_{\gamma_y} \to -\frac{2\sqrt{\hat{k}_x}}{\left(1+\sqrt{\hat{k}_x}\right)^2}, \quad \gamma_i \to \infty, \quad \hat{k}_x > 1. \tag{40}$$

These limits are important for the homeostasis of platelets abundance where there is strong evidence for $\gamma_i/\gamma_y \gg 1$ [28]. While there is no evidence for induced decay in the Hsp-Hsf feedback circuit, our analysis shows that in the case of $\gamma_i = 0$, sensitivity reduction can occur from -1 to $-1/2$ (Fig. 5) making $y^*_T \propto 1/\sqrt{\gamma_y}$.

Analysis of the sequestration-based feedback considering stochasticity of biochemical reactions and transcriptional bursting shows a noise reduction in the feedback system compared to no feedback (i.e., no binding between X_f and Y_f) in the absence of induced decay ($\gamma_i = 0$). Importantly, noise further attenuates with increasing γ_i (Fig. 6). While this investigation relies on stochastic simulation of the underlying biochemical reactions, future work will use analytical tools based on moment closure schemes [62]–[64] to systematically investigate noise properties, specifically focusing on the origin of local minima in the Fano factor (Fig. 6).

APPENDIX

Taking the derivative of (7) we obtain

$$\begin{aligned}\frac{\partial c(x_T,y_T)(x_T,y_T)}{\partial x_T} &= \frac{1}{2}\left(1-\frac{k_d+x_T-y_T}{\sqrt{(k_d+x_T+y_T)^2-4x_Ty_T}}\right)\\ &= \frac{1}{2}\left(1-\frac{k_d+x_T-y_T}{\sqrt{(k_d+x_T-y_T)^2+4k_dy_T}}\right)\end{aligned} \tag{41}$$

Note that while k_d, y_T, x_T only take positive real values, $k_d + x_T - y_T$ can be either negative or positive depending on the total abundances of TPO and platelets. However, irrespective of the sign of $k_d + x_T - y_T$

$$-1 \leq \frac{k_d+x_T-y_T}{\sqrt{(k_d+x_T-y_T)^2+4k_dy_T}} \leq 1 \tag{42}$$

which from (41) implies that

$$0 \leq \frac{\partial c(x_T,y_T)(x_T,y_T)}{\partial x_T} \leq 1. \tag{43}$$

REFERENCES

[1] U. Alon, *An Introduction to Systems Biology: Design Principles of Biological Circuits*. Chapman and Hall/CRC, 2011.

[2] N. Rosenfeld, M. B. Elowitz, and U. Alon., "Negative autoregulation speeds the response times of transcription networks." *Journal of Molecular Biology*, vol. 323, pp. 785–793, 2002.

[3] K. R. Ghusinga, J. J. Dennehy, and A. Singh, "First-passage time approach to controlling noise in the timing of intracellular events," *Proceedings of the National Academy of Sciences*, vol. 114, pp. 693–698, 2017.

[4] R. Murugan and G. Kreiman, "On the minimization of fluctuations in the response times of autoregulatory gene networks," *Biophysical Journal*, vol. 101, pp. 1297–1306, 2011.

[5] A. Becskei and L. Serrano, "Engineering stability in gene networks by autoregulation," *Nature*, vol. 405, pp. 590–593, 2000.

[6] A. Singh, "Negative feedback through mRNA provides the best control of gene-expression noise," *IEEE Transactions on Nanobioscience*, vol. 10, pp. 194–200, 2011.

[7] Y. Tao, X. Zheng, and Y. Sun, "Effect of feedback regulation on stochastic gene expression," *Journal of Theoretical Biology*, vol. 247, pp. 827–836, 2007.

[8] S. Hooshangi and R. Weiss, "The effect of negative feedback on noise propagation in transcriptional gene networks," *CHAOS*, vol. 16, 2006.

[9] Y. Dublanche, K. Michalodimitrakis, N. Kummerer, M. Foglierini, and L. Serrano, "Noise in transcription negative feedback loops: simulation and experimental analysis," *Molecular Systems Biology*, vol. 2, p. 41, 2006.

[10] A. Singh and J. P. Hespanha, "Optimal feedback strength for noise suppression in autoregulatory gene networks," *Biophysical Journal*, vol. 96, pp. 4013–4023, 2009.

[11] N. Kumar, T. Platini, and R. V. Kulkarni, "Exact Distributions for Stochastic Gene Expression Models with Bursting and Feedback," *Physical Review Letters*, vol. 113, p. 268105, 2014.

[12] M. Voliotis and C. G. Bowsher, "The magnitude and colour of noise in genetic negative feedback systems," *Nucleic Acids Research*, 2012.

[13] A. Milias-Argeitis, S. Summers, J. Stewart-Ornstein, I. Zuleta, D. Pincus, H. El-Samad, M. Khammash, and J. Lygeros, "In silico feedback for in vivo regulation of a gene expression circuit," *Nature Biotechnology*, vol. 29, 2011.

[14] I. Lestas, G. Vinnicombegv, and J. Paulsson, "Fundamental limits on the suppression of molecular fluctuations," *Nature*, vol. 467, pp. 174–178, 2010.

[15] D. Nevozhay, R. M. Adams, K. F. Murphy, K. Josic, and G. Balazsi, "Negative autoregulation linearizes the dose response and suppresses the heterogeneity of gene expression," *Proceedings of the National Academy of Sciences*, vol. 106, pp. 5123–5128, 2009.

[16] E. J. Hancock, J. Ang, A. Papachristodoulou, and G.-B. Stan, "The interplay between feedback and buffering in cellular homeostasis," *Cell systems*, vol. 5, no. 5, pp. 498–508, 2017.

[17] A. Singh and J. P. Hespanha, "Stochastic analysis of gene regulatory networks using moment closure," in *Proc. of the 2007 Amer. Control Conference, New York, NY*, 2006.

[18] S. Modi, S. Dey, and A. Singh, "Noise suppression in stochastic genetic circuits using pid controllers," *PLoS Computational Biology*, vol. 17, no. 7, p. e1009249, 2021.

[19] Z. Vahdat, K. Nienałtowski, Z. Farooq, M. Komorowski, and A. Singh, "Information processing in unregulated and autoregulated gene expression," in *2020 European Control Conference (ECC)*. IEEE, 2020, pp. 258–263.

[20] X. Zhou, R. A. Franklin, M. Adler, J. B. Jacox, W. Bailis, J. A. Shyer, R. A. Flavell, A. Mayo, U. Alon, and R. Medzhitov, "Circuit design features of a stable two-cell system," *Cell*, vol. 172, no. 4, pp. 744–757, 2018.

[21] R. H. Gomer, W. Jang, and D. Brazill, "Cell density sensing and size determination," *Development, growth & differentiation*, vol. 53, no. 4, pp. 482–494, 2011.

[22] D. A. Brock, R. D. Hatton, D.-V. Giurgiutiu, B. Scott, W. Jang, R. Ammann, and R. H. Gomer, "Cf45-1, a secreted protein which participates in dictyostelium group size regulation," *Eukaryotic cell*, vol. 2, no. 4, pp. 788–797, 2003.

[23] S. Modi and A. Singh, "Controlling organism size by regulating constituent cell numbers," in *2018 IEEE Conference on Decision and Control (CDC)*, 2018, pp. 2685–2690.

bioRxiv preprint doi: https://doi.org/10.1101/2022.03.26.485894; this version posted March 27, 2022. The copyright holder for this preprint (which was not certified by peer review) is the author/funder, who has granted bioRxiv a license to display the preprint in perpetuity. It is made available under aCC-BY-ND 4.0 International license.

[24] R. Formisano, K. D. Rosikon, A. Singh, and H. S. Dhillon, "The dopamine membrane transporter plays an active modulatory role in synaptic dopamine homeostasis," *Journal of neuroscience research*, 2021.

[25] R. Formisano, M. D. Mersha, J. Caplan, A. Singh, C. H. Rankin, N. Tavernarakis, and H. S. Dhillon, "Synaptic vesicle fusion is modulated through feedback inhibition by dopamine auto-receptors," *Synapse*, vol. 74, no. 1, p. e22131, 2020.

[26] S. W. Fong, I. S. McLennan, A. McIntyre, J. Reid, K. I. Shennan, and G. S. Bewick, "Tgf-β2 alters the characteristics of the neuromuscular junction by regulating presynaptic quantal size," *Proceedings of the National Academy of Sciences*, vol. 107, no. 30, pp. 13 515–13 519, 2010.

[27] B. Kiragasi, P. Goel, S. Perry, Y. Han, X. Li, and D. Dickman, "The auxiliary glutamate receptor subunit dsol-1 promotes presynaptic neurotransmitter release and homeostatic potentiation," *Proceedings of the National Academy of Sciences*, vol. 117, no. 41, pp. 25 830–25 839, 2020.

[28] J. J. Feher, *Quantitative human physiology: an introduction*. Academic press, 2017.

[29] Y. Kheifetz and M. Scholz, "Modeling individual time courses of thrombopoiesis during multi-cyclic chemotherapy," *PLoS computational biology*, vol. 15, no. 3, p. e1006775, 2019.

[30] K. Kaushansky *et al.*, "The molecular mechanisms that control thrombopoiesis," *The Journal of clinical investigation*, vol. 115, no. 12, pp. 3339–3347, 2005.

[31] H. El-Samad, H. Kurata, J. Doyle, C. Gross, and M. Khammash, "Surviving heat shock: control strategies for robustness and performance," *Proceedings of the National Academy of Sciences*, vol. 102, no. 8, pp. 2736–2741, 2005.

[32] Z. A. Feder, A. Ali, A. Singh, J. Krakowiak, X. Zheng, V. P. Bindokas, D. Wolfgeher, S. J. Kron, and D. Pincus, "Subcellular localization of the j-protein sis1 regulates the heat shock response," *Journal of Cell Biology*, vol. 220, no. 1, 2021.

[33] S. W. Kmiecik, L. Le Breton, and M. P. Mayer, "Feedback regulation of heat shock factor 1 (hsf1) activity by hsp70-mediated trimer unzipping and dissociation from dna," *The EMBO journal*, vol. 39, no. 14, p. e104096, 2020.

[34] J. E. Pérez-Ortín, A. Mena, M. Barba-Aliaga, A. Singh, S. Chávez, and J. García-Martínez, "Cell volume homeostatically controls the rdna repeat copy number and rrna synthesis rate in yeast," *PLoS genetics*, vol. 17, no. 4, p. e1009520, 2021.

[35] T. G. Minchington, S. Griffiths-Jones, and N. Papalopulu, "Dynamical gene regulatory networks are tuned by transcriptional autoregulation with microrna feedback," *Scientific reports*, vol. 10, no. 1, pp. 1–13, 2020.

[36] J. Tsang, J. Zhu, and A. van Oudenaarden, "MicroRNA-mediated feedback and feedforward loops are recurrent network motifs in mammals," *Molecular Cell*, vol. 26, pp. 753–767, 2007.

[37] C. Briat, C. Zechner, and M. Khammash, "Design of a synthetic integral feedback circuit: dynamic analysis and dna implementation," *ACS synthetic biology*, vol. 5, no. 10, pp. 1108–1116, 2016.

[38] N. Olsman, A.-A. Baetica, F. Xiao, Y. P. Leong, R. M. Murray, and J. C. Doyle, "Hard limits and performance tradeoffs in a class of antithetic integral feedback networks," *Cell systems*, vol. 9, no. 1, pp. 49–63, 2019.

[39] C. Briat, A. Gupta, and M. Khammash, "Antithetic integral feedback ensures robust perfect adaptation in noisy biomolecular networks," *Cell systems*, vol. 2, no. 1, pp. 15–26, 2016.

[40] A.-A. Baetica, Y. P. Leong, and R. M. Murray, "Guidelines for designing the antithetic feedback motif," *Physical Biology*, vol. 17, no. 5, p. 055002, 2020.

[41] B. Shannon, C. G. Zamora-Chimal, L. Postiglione, D. Salzano, C. S. Grierson, L. Marucci, N. J. Savery, and M. Di Bernardo, "In vivo feedback control of an antithetic molecular-titration motif in escherichia coli using microfluidics," *ACS Synthetic Biology*, vol. 9, no. 10, pp. 2617–2624, 2020.

[42] S. K. Aoki, G. Lillacci, A. Gupta, A. Baumschlager, D. Schweingruber, and M. Khammash, "A universal biomolecular integral feedback controller for robust perfect adaptation," *Nature*, vol. 570, no. 7762, pp. 533–537, 2019.

[43] N. Barkai and S. Leibler, "Robustness in simple biochemical networks," *Nature*, vol. 387, no. 6636, pp. 913–917, 1997.

[44] Z. Sun, W. Wei, M. Zhang, W. Shi, Y. Zong, Y. Chen, X. Yang, B. Yu, C. Tang, and C. Lou, "Synthetic robust perfect adaptation achieved by negative feedback coupling with linear weak positive feedback," *Nucleic Acids Research*, vol. 50, no. 4, pp. 2377–2386, 2022.

[45] D. K. Agrawal, R. Marshall, V. Noireaux, and E. D. Sontag, "In vitro implementation of robust gene regulation in a synthetic biomolecular integral controller," *Nature communications*, vol. 10, no. 1, pp. 1–12, 2019.

[46] J. E. Ferrell Jr, "Perfect and near-perfect adaptation in cell signaling," *Cell systems*, vol. 2, no. 2, pp. 62–67, 2016.

[47] M. Lebois and E. C. Josefsson, "Regulation of platelet lifespan by apoptosis," *Platelets*, vol. 27, no. 6, pp. 497–504, 2016.

[48] K. A. Aas and F. H. Gardner, "Life span of normal human platelets tagged with chromium51," in *International Society of Blood Transfusion*, 1958, vol. 7, pp. 364–368.

[49] F. G. Pluthero and W. H. Kahr, "The birth and death of platelets in health and disease," *Physiology*, vol. 33, no. 3, pp. 225–234, 2018.

[50] H. K. Khalil, *Nonlinear Systems*. Pearson, 2002.

[51] S. Chong, C. Chen, H. Ge, and X. S. Xie, "Mechanism of transcriptional bursting in bacteria," *Cell*, vol. 158, pp. 314–326, 2014.

[52] D. M. Suter, N. Molina, D. Gatfield, K. Schneider, U. Schibler, and F. Naef, "Mammalian genes are transcribed with widely different bursting kinetics," *Science*, vol. 332, pp. 472–474, 2011.

[53] L. C. R. Fraser, R. J. Dikdan, S. Dey, A. Singh, and S. Tyagi, "Reduction in gene expression noise by targeted increase in accessibility at gene loci," *Proceedings of the National Academy of Sciences*, vol. 118, no. 42, p. e2018640118, 2021.

[54] A. Singh, B. S. Razooky, R. D. Dar, and L. S. Weinberger, "Dynamics of protein noise can distinguish between alternate sources of gene-expression variability," *Molecular Systems Biology*, vol. 8, p. 607, 2012.

[55] N. Kumar, A. Singh, and R. V. Kulkarni, "Transcriptional bursting in gene expression: Analytical results for genera stochastic models," *PLOS Computational Biology*, vol. 11, p. e1004292, 2015.

[56] A. Raj, C. Peskin, D. Tranchina, D. Vargas, and S. Tyagi, "Stochastic mRNA synthesis in mammalian cells," *PLOS Biology*, vol. 4, p. e309, 2006.

[57] N. Van Kampen, *Stochastic Processes in Physics and Chemistry*. Elsevier, 2011.

[58] D. T. Gillespie, "A general method for numerically simulating the stochastic time evolution of coupled chemical reactions," *Journal of Computational Physics*, vol. 22, pp. 403–434, 1976.

[59] C. C. Samaniego and E. Franco, "Ultrasensitive molecular controllers for quasi-integral feedback," *Cell Systems*, vol. 12, no. 3, pp. 272–288, 2021.

[60] M. Chevalier, M. Gómez-Schiavon, A. H. Ng, and H. El-Samad, "Design and analysis of a proportional-integral-derivative controller with biological molecules," *Cell Systems*, vol. 9, no. 4, pp. 338–353, 2019.

[61] Y. Qian and D. Del Vecchio, "Realizing 'integral control' in living cells: how to overcome leaky integration due to dilution?" *Journal of The Royal Society Interface*, vol. 15, no. 139, p. 20170902, 2018.

[62] K. R. Ghusinga, C. A. Vargas-Garcia, A. Lamperski, and A. Singh, "Exact lower and upper bounds on stationary moments in stochastic biochemical systems," *Physical Biology*, vol. 14, p. 04LT01, 2017.

[63] S. Modi, M. Soltani, and A. Singh, "Linear noise approximation for a class of piecewise deterministic markov processes," *American Control Conference (ACC)*, 2018.

[64] A. Singh and J. P. Hespanha, "Models for multi-specie chemical reactions using polynomial stochastic hybrid systems," in *IEEE Conference on Decision and Control*, 2005.